Open Access Journal

Journal of Power Technologies 96 (2) (2016) 137–144

journal homepage:papers.itc.pw.edu.pl

Numerical Study of a Hybrid Photovoltaic Power Supply System

Abdelkader Gourbi[a,*], Imen Bousmaha[a], Mostefa Brahami[a], Amar Tilmatine[b]

[a] *ICEPS laboratory, Djillali Liabes University of Sidi Bel Abbes, Algeria*
[b] *APELEC Laboratory, Djillali Liabes University of Sidi Bel Abbes*

Abstract

This paper aims to analyze a hybrid photovoltaic system for production of electrical energy associated with a storage system to be employed in an isolated site. Mathematical models were proposed describing the physical operation of each part of the studied system, according to the meteorological conditions or the estimated data. Then programs developed with Matlab software were carried out to simulate the influence of various parameters on each element of the conversion chain. The results obtained have shown a good and accurate simulation of the energy behavior of the complete system and can be used to give answers to many questions about this type of installation and to help manufacturers make the right decisions.

Keywords: Photovoltaic hybrid systems, Renewable energy, Diesel, battery storage system, Modeling and simulation,

1. Introduction

Renewable energy is currently considered as one of the most efficient solutions to the energy problems in the world. Among the several renewable energy sources there are wind, marine, oceanic flows, geothermal, solar and photovoltaic. This latter has many advantages: nonpolluting, free, silent, no rotating parts, independent dimensions. However, purely photovoltaic systems associated with a storage battery face major variation in terms of production due to the intermittent time conditions and it must be oversized to supply all types of loads with sufficient reliability, but the investment costs will be in consequence higher.

The PV generator interconnection with other energy sources (wind, diesel fuel, hydroelectric) in a Hybrid Energy System (HES) can have a beneficial impact on the production of electrical energy in terms of cost and availability.

The first hybrid power systems village comprising a PV and a diesel generator was installed on December 16, 1978 in Papago Indian Village, Schuchuli, Arizona, USA. The power produced by the system was used to provide electricity for the community's needs: refrigerator, washing machine, sewing machine, water pumps and lights, until an electric grid was extended to the village in 1983 [1, 2].

Research on Hybrid Power Systems based on renewable sources started about 30 years ago. The first papers appeared in the mid-eighties [3], but literature on hybrid systems did not blossom until the early 1990s [4].

*Corresponding author
Email address: aekett@yahoo.fr (Abdelkader Gourbi)

The publications dedicated to photovoltaic hybrid systems with conventional source, present the results from existing and installed systems [5–7], while others examine the possibility of adding photovoltaic panels as a source of additional energy in existing conventional source installations [8–10]. Other authors conducted theoretical studies on the analysis of processes taking place within the system [11, 12], the optimization of the hybrid system design [13, 14], or the energy management strategy [15]. Many works have been performed by using commercial software such as HOMER [16], Hybrid2 [12], LabVIEW [13] and most publications on these systems use a diesel generator as a conventional energy source.

In order to make new contributions to hybrid photovoltaic systems, this paper is aimed at the elaboration of mathematical models for the various components of a pilot hybrid system comprising a photovoltaic generator, a diesel generator and a storage system. Modeling each section retrieves by simulation the influence of the parameters on the characteristics of the various elements of the conversion chain. Due to the random nature of meteorological conditions and the consumer profile, one needs to get information on how the system operates in different situations and times.

2. Description of the analyzed system

A hybrid renewable energy system is an electrical system having more than one power source, of which at least one is renewable. The hybrid system may include a storage de-

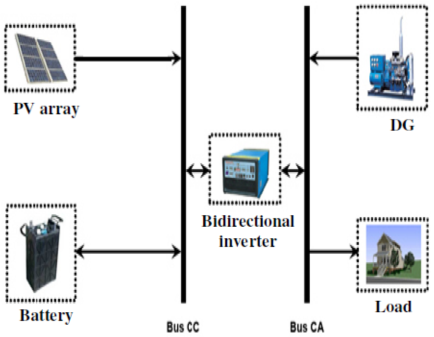

Figure 1: The analyzed hybrid system with a diesel generator DG

vice and can operate in standalone mode or grid connected mode [17, 18].

The system to be modeled is composed of the following equipments as shown in Fig 1:

- A photovoltaic generator
- A diesel generator
- A storage system
- An inverter
- An electrical load

In this work, we opted for the parallel configuration because it offers more advantages compared to other configurations [19, 20], in which the system works in standalone mode and has to supply an average load of 4600 Wh/d.

Using the parallel configuration shown in Fig. 1, all energy sources may supply the load separately at low or medium load demand, as well as to supply peak loads from combined sources by synchronizing the inverter with the alternator output waveform. The bi-directional inverter can charge the battery bank (rectifier) when excess energy is available from the diesel generator, and can function as a DC-AC converter (inverter) under normal operation. The bi-directional inverter may provide peak shaving as part of the control strategy when the diesel generator is overloaded [20].

The technical data of each component of the analyzed system are presented in table 1.

3. Mathematical equations

The intermittent nature of renewable energy sources and its randomness and the large number of system configurations and equipment contribute to complicate the design and operation process of the hybrid system. Consequently, the models need to be defined to simulate the complex behavior of these composite systems.

In this section we present the models of each element of the system described in the previous section.

Table 1: Technical data of each component

Designations	Data
PV	
Model	BP-3125
Number of panels	12
Connection Mode	6 of 2 series
Number of cells n_s	36
maximum power P_{mp} in STC*, W	125
Short current –Circuit I_{scn} in STC*, A	7.54
Open circuit voltage V_{ocn} in STC*, V	22.1
current at maximum power Imp in STC*, A	7.1
voltage at maximum power V_{mp} in STC*, V	17.6
Temperature coefficient of I_{sc} ki, %/°C	0.065
Temperature coefficient of V_{oc} k_v, mV/°C	–80
Batteries	
electromotive force E, V	2
number of series cells	12
C10 capacity, Ah	1000
Rated voltage V_{batn}, V	24
initial State Of Charge SOC, %	100
Generator	
Rated power P_n, kW	6.6
fuel	Diesel
Inverter	
Inverter rated power P_{inv}, kW	2.3
Maxeff, %	95
Load	
average load, Wh	4600

*The Standard testing conditions to measure photovoltaic cells or modules nominal output power. Irradiation level is 1000 W/m^2, with the reference air mass 1.5 solar spectral irradiation distribution and cell or module junction temperature of 25°C.

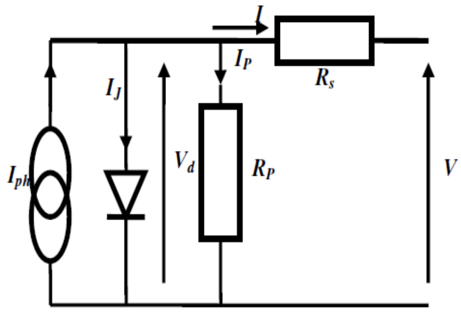

Figure 2: The Equivalent electrical circuit of a photovoltaic cell

3.1. PV generator Model

Singer model was used for modeling the PV generator [21].

This model is based on an equivalent circuit of a photovoltaic cell (Fig. 2) which comprises a current source that models the conversion of light flux into electrical energy, a shunt resistance Rp representing the surface quality along the cell periphery, a series resistance Rs which arises from the ohmic contact between metal and semiconductor internal resistance and a parallel diode which models the PN junction [22–29].

The current I generated by the cell is given by Kirchhoff's law:

$$I = I_{ph} - I_j - I_p \tag{1}$$

The current I_p flowing in the shunt resistor and the junction current I_j are given by equations (2) and (3) respectively.

$$I_p = \frac{V + IR_s}{R_p} \tag{2}$$

$$I_j = I_0\left[\exp\left[\frac{q(V+IR_s)}{AkT}\right]-1\right] \quad (3)$$

with I_0: saturation current of the diode (A). A: diode ideality factor dependence on PV technology =1.3 for polycrystalline silicon solar cell. k: Boltzmann's constant (J/K). T: temperature of the cell (K). q: electron charge (C). V: voltage at the terminals of the cell.

By replacing (2) and (3) into (1) we obtain:

$$I = I_{ph} - I_0\left[\exp\left[\frac{q(V+IR_s)}{AkT}\right]-1\right] - \left[\frac{V+IR_s}{R_p}\right] \quad (4)$$

For a photovoltaic module of ns series cells, the equation (4) becomes:

$$I = I_{ph} - I_0\left[\exp\left[\frac{q(V+IR_s)}{n_sAkT}\right]-1\right] - \left[\frac{V+IR_s}{R_p}\right] \quad (5)$$

Where: I, I_{ph}, I_o, V, R_s, R_p are the parameters of a photovoltaic panel.

Moreover, the current I_{ph} generated by the light is:

$$I_{ph} = \left(\frac{R_s+R_p}{R_p}\right)Isc_n\left[\left(1+\frac{k_i}{100}(T-T_n)\right)\frac{G}{G_n}\right] \quad (6)$$

The diode saturation current I_0 may be expressed by [22, 24, 26]:

$$I_0 = \frac{Isc_n\left(1+\frac{k_i}{100}(T-T_n)\right)}{\left[\exp\left((Voc_n+k_v(T-T_n))\,q/n_sAKT\right)-1\right]} \quad (7)$$

where: Isc_n—the short-circuit current in STC, A; Voc_n—the Open circuit voltage in STC, V; T and T_n being the actual and STC temperatures, K, respectively; G (W/m^2) is the Irradiation on the PV panel surface, and G_n is the STC irradiation.

For a PV generator of Nss. Series x Npp parallel panels Equation (5) becomes:

$$I_G = N_{pp}\cdot I_{ph} - N_{pp}\cdot I_0\left[\exp\left[\frac{q(V+IR_s\cdot(N_{ss}/N_{pp}))}{n_sAkT}\cdot N_{ss}\right]-1\right] - \left[\frac{(V+IR_s\cdot(N_{ss}/N_{pp}))\cdot N_{ss}}{R_p\cdot(N_{ss}/N_{pp})}\right] \quad (8)$$

The generator power is given by the following equation:

$$P_{pv} = I_G\cdot V \quad (9)$$

3.2. Storage Battery Model

CIEMAT model was used for modeling the storage battery [30, 31]. This model is based on the electrical diagram presented in Fig. 3, according to which the battery is described with two elements only (whose characteristics depend on a set of parameters): the voltage source and the internal resistance.

For the n_b series cells, the following equation of the battery voltage is used:

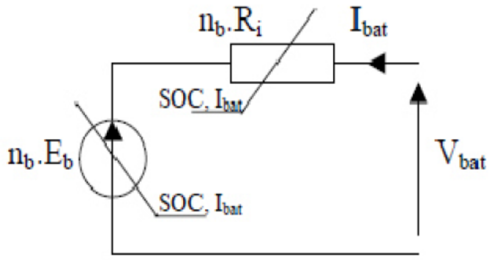

Figure 3: Equivalent electrical diagram of n_b battery elements in series

$$V_{bat} = n_b\cdot E_b + n_b\cdot R_i\cdot I_{batt} \quad (10)$$

where V_{bat} and I_{bat} are the battery voltage and current (according to the receptor convention), E_b is the electromotive force which depends on the battery state of charge (denoted SOC), and R_i is the internal resistance of an element.

The capacity model yields the quantity of energy C_{bat} that the battery can restore, according to the average discharge current $I_{bat.ave}$ [30, 31]. The corresponding expression is established beginning with the I_{10} current, relative to operating mode C_{10} (with this value representing battery capacity over a discharge regime at constant current during 10 hours: $C_{10} = 10\,.\,I_{10}$).

$$\frac{C_{bat}}{C_{10}} = \frac{1.67}{1+0.67\cdot\left(\frac{I_{bat.ave}}{I_{10}}\right)}\cdot(1+0.005+\Delta T) \quad (11)$$

where ΔT is the accumulator heating assumed to be identical for all elements and calculated with respect to the reference ambient temperature of 25°C. C_{bat} is used as a reference to determine battery SOC, which will then be formulated according to the quantity of lacking battery charge, Q_{bat}.

$$SOC = 1 - \frac{Q_{bat}}{C_{bat}} \quad (12)$$

The temporal evolution of "Q_{bat}" depends on the battery operation (increases in discharge mode and vice versa). The estimation of Q_{bat} is carried out by using Coulomb law:

$$Q_{bat} = I_{bat}\cdot t \quad (13)$$

where: "t " is the battery operating duration with a current "I_{bat}".

The expression for battery voltage has been derived from Equation (11) above as a function of its charge (index "c") or discharge (index "d") regime. This set-up thereby leads to a structure tied to both of the battery's internal elements: the electromotive force and the internal resistance [30–32]:

$$V_d = n_b\cdot(2.085-0.12\cdot(1-SOC)) - n_b\frac{|I_{bat}|}{C_{10}}\cdot\left[\frac{4}{|I_{bat}^{1.3}|}+\frac{0.27}{(SOC)^{1.5}}+0.02\right]\cdot(1-0.007\cdot\Delta T \quad (14)$$

$$V_c = n_b\cdot(2+0.16\cdot SOC) + n_b\frac{|I_{bat}|}{C_{10}}\cdot\left[\frac{6}{1+I_{bat}^{0.86}}+\frac{0.48}{(1-SOC)^{1.2}}+0.036\right]\cdot(1-0.025\cdot\Delta T) \quad (15)$$

3.3. Diesel Generator Model

The diesel generator (DG) is a diesel engine coupled to a synchronous generator. This system includes a speed control on the diesel engine that operates by adjusting the fuel flow in order to maintain constant the engine rotation speed and the electrical frequency at the generator output. The frequency of the network is directly related to the generator rotation speed and is therefore maintained at the desired level [33].

In a hybrid system, the DG can generate the rated power requested by the load while the excess energy will be used to charge the batteries.

The energy produced by a DG is expressed as follows [34]:

$$E_{DG} = P_n \cdot \eta_{ge} \cdot t \tag{16}$$

where: η_{ge}—the DG efficiency, t—the DG operating duration, P_n—the DG rated output power.

A diesel generator is generally characterized by its fuel consumption (hourly in l/h or specific in l/kWh). The diesel generator hourly consumption can be expressed as follows [35]:

$$q(t) = a \cdot P_{ge}(t) + b \cdot P_n \tag{17}$$

where "a" (l/kWh) and "b" (l/kWh) are the constant characteristics of the diesel generator, P_{ge} (kW) is the diesel generator power generated at a given time t and P_n (kW) is the rated generator power [35–37].

The coefficients obtained for our generator are: $a = 0.245$ (l/kWh) and $b = 0.0689$ (l/kWh) with a coefficient of determination (R^2) equal to 0.996.(these coefficients were obtained through the statistical method of least-squares [38] based on the experimental data given by the manufacturer in the data sheet of the diesel generator : fuel consumption at 100% of $P_n = 2.08$ l/h, at 75% of $P_n = 1.65$ l/h, at 50% of $P_n = 1.29$ l/h, at 25% of $P_n = 0.85$ l/h).

3.4. Converter Model

The inverters are static converters which enable an AC voltage source (at the output) to be obtained from a DC voltage source (at the input) [36].

The inverters are characterized by their efficiency, which is a function of the delivered output power and is given by the following expression:

$$\eta_{inv} = \frac{1}{1 + \frac{\Delta P}{P_s}} \tag{18}$$

where: ΔP—inverter losses, P_s—inverter power output.

3.5. Load model

There are two types of load consumption:

Constant load: the power variation as a function of time is a straight line,

Variable Load: is represented by the variable and continuous demand during the day, the month or during the year.

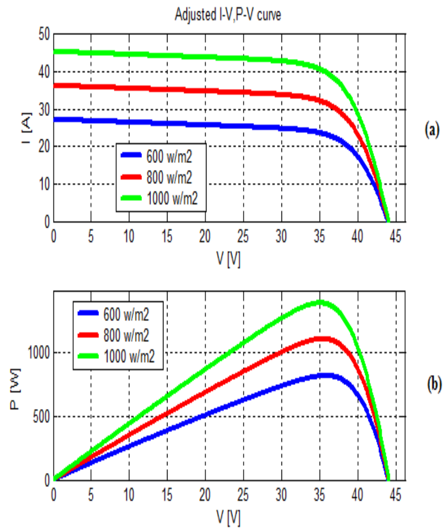

Figure 4: I–V and P–V curves of a PV generator at variable irradiation and constant temperature

The electrical power delivered by the system to the user is that which is delivered by the inverter to the load (P_s) plus the diesel generator power (if necessary):

$$P_{sys} = P_s + P_{ge} \tag{19}$$

Total system efficiency is determined by the following equation:

$$\eta_{sys} = \eta_{Pv} \times \eta_{bat} \times \eta_{inv} \times \eta_{ge} \tag{20}$$

4. Results and discussion

Using the mathematical models proposed in the previous section, a simulation program of the entire conversion chain of the hybrid system was developed using Matlab software.

For the PV, Newton-Raphson numerical method [39] was used to solve similar equations to expression (8) (I = f (I, V)), and then estimate the power by means of equation (9). The values of Rs and Rp are determined using the method described in [22]. Moreover, for the battery and the other components, we used the simple equations presented above.

The I–V and P–V curves at variable irradiation and temperature obtained by using our model are represented in Figs 4 and 5.

According to the obtained results in Fig. 4, one can see that at fixed temperature (25°C), the short-circuit current decreases with respect to the irradiation, while the value of the open circuit voltage is maintained constant (Fig. 4.a) and the optimum operating point moves on an almost straight horizontal line (Fig. 4.b). On the other hand, at fixed irradiation (1000 W/m^2), a decrease of the temperature causes an increase of the open circuit voltage and a smaller degradation of the short-circuit current (Fig. 5.a). Consequently,

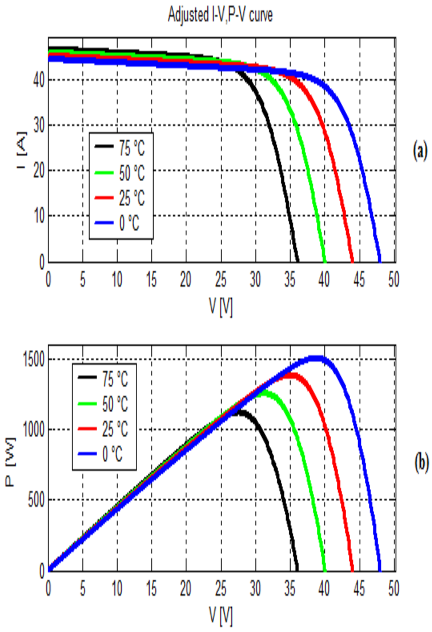

Figure 5: I–V and P–V curves of a PV generator at variable temperature and constant irradiation

the PV generator performs a better operation (high electrical efficiency and high power output) in a low-temperature rather than a high-temperature environment (Fig. 5.b).These results are in accordance with the experimental results published by many authors in this field [21–29].

Moreover, the results show that the P-V characteristic of the PV generator is nonlinear and changes with irradiation and temperature. There is a point on the V-P or V-I characteristic, called the Maximum Power Point (MPP), at which the PV generator operates with maximum efficiency and produces its maximum output power. Moreover, using a MPPT controller serves to improve the performance of the PV generator [40]. The Maximum Power Point Tracking (MPPT) techniques are used to maintain the PV generator operating point at its MPP. Therefore, this technique is of great importance for maximizing the energy produced by the PV generator. This will increase the penetration of renewable energy source in the entire hybrid system.

Figs 6–8 show the simulation results related to the influence of the temperature on the capacity, state of charge (SOC) and the battery voltage for three different values of the temperature (25, 40 and 50°C).

As seen in Fig. 6, the capacity decreases as the discharge current is increased, this is mainly due to the internal resistance of the battery (Peukert Effect).This latter increases during discharging mode because there is less reactive product in the electrolyte. Thus, if the discharge current increases, the capability and the discharge duration decrease. So the more slowly the battery is discharged, the more it is able to provide the necessary energy for the hybrid system.

Moreover, the increase in temperature causes a moderate rise in the storage capacity. The capacity reaches its mini-

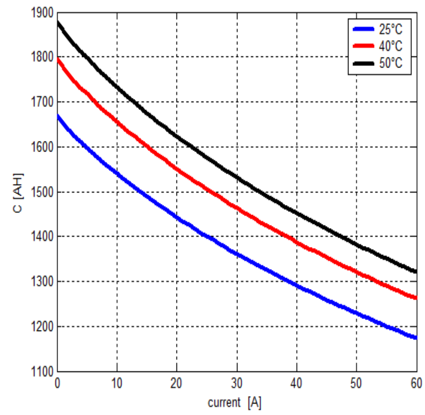

Figure 6: Variation of the capacity versus the current for different values of the temperature

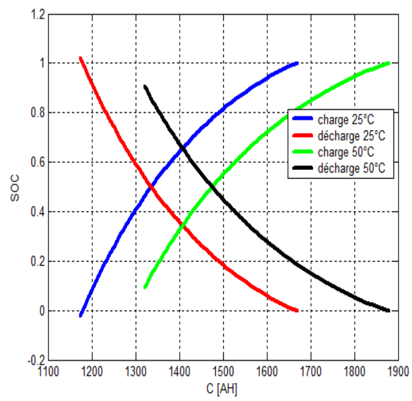

Figure 7: Variation of the SOC versus the capacity for different values of temperature

mum of 1650 Ah at 25°C while it increases up to 1900 Ah at a temperature of 50° C. When the temperature increases the internal resistance of the battery lowers since the ion mobility in the electrolyte increases with temperature and therefore the capacity increases [30].

Therefore, it's highly recommended that the manufacturers and the installers of such systems take into consideration the climate (temperature) of the site and the application (load profile) for which the various pieces of equipment are intended in order to obtain a maximum efficiency.

Fig. 7 represents the variation of the SOC versus the capacity for different values of temperature.

For the same capacity of 1500 Ah for instance, in the case of the charge mode, temperature increase causes SOC to decrease: at 25°C SOC is equal to 80%, while it decreases to 55% at 50°C.However, in the case of the discharge mode, a temperature rise is followed by an increase in SOC: SOC is equal to 20% at 25°C and increases to 40% at 50°C.

On the other hand, when the charge rate increases by increasing either the operating duration "h" or the current "A", i.e. the capacity "Ah", the SOC increases and vice versa.

These conditions can lead, in the framework of battery maintenance, to a better monitoring in the studied site and a better optimization.

Figs 8.a and 8.b show the variation of current versus the voltage for different values of temperature for both cases of charge and discharge respectively.

For the same current of 50 A for example, in the charge mode (Fig. 8.a), the battery voltage decreases with temperature (V= 28 V at 25°C and V= 26 Vat 50°C).On other hand, in the case of the discharge mode (Fig. 8.b), the battery voltage increases with the temperature (V= 22 V at 25°C while V=23 V at 50°C).

Consequently, the battery voltage plots are affected by temperature as is the SOC, for both cases of charge and discharge modes.

Thus, since the SOC of the batteries depends on their voltage, it is used as an indication parameter in the battery charge controllers. During the charging phase, the solar charge controller needs to know when the battery is fully charged to ensure timely protection against overcharging. When discharging the battery, it is also important to know the state of charge in order to ensure protection of the battery against harmful deep discharge. Therefore, there are various criteria which can indicate the charge level of the battery at any time. Some of these criteria are better suited than others, and the simplest and most common one is the battery voltage. With this method, a fixed charge cut-off voltage is defined. When this voltage is reached, charging is stopped. A fixed deep discharge threshold is also defined. If the battery voltage falls below this value, the load is switched off. This method is simple, since the voltage of the battery is easy to measure precisely.

Using this method, a fixed voltage of end charging is defined. When this voltage is reached, charging is stopped. Moreover, a fixed deep discharge voltage is also set. If the battery voltage falls below this value, the load is disconnected. This method is simple, since the voltage of the battery is easy to measure accurately.

Fig. 9 shows the efficiency of the inverter as a function of the power demand P_s for 2 different values of power losses.

We note that efficiency decreases with increasing losses, and the inverter must operate near its rated power for better performance.

There are several factors which affect the inverter losses:

Own inverter loss: due to its components, such as the transformer, the semiconductor material, the resistance and other components.

Temperature inverter loss: Inverters, like all semiconductor-based equipment, are sensitive to overheating and, in general, operate better at cooler temperatures, while power losses and damage occur at higher internal temperatures.

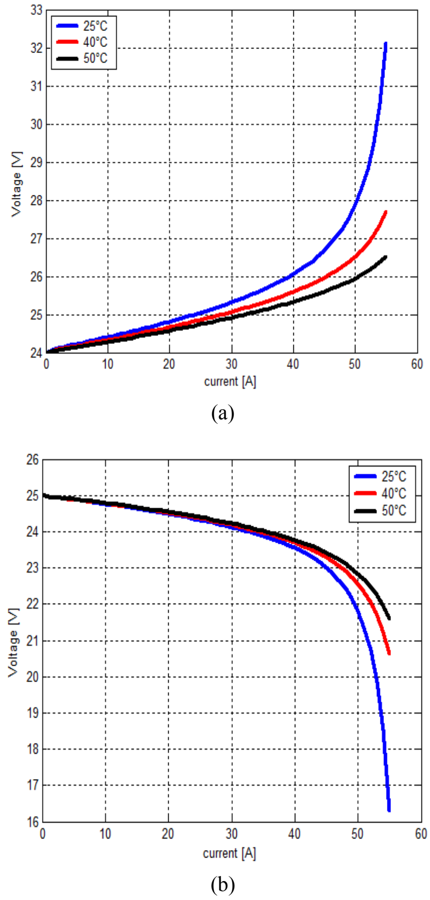

Figure 8: Variation of the voltage versus the current for different values of temperature: a) discharge mode; b) charging mode

Inverter Loss due to the power threshold': when the power of the PV (or battery) is not sufficient to start the inverter.

Inverter Loss due to power overcharging; when the MPP power is higher than the input power required for obtaining the specified P_{inv} (AC), the inverter displaces the operating point on the I-V curve in order to obtain exactly the power required for P_{inv} (AC). This loss value represents the difference between P_{mp} and this adjusted power. The displacement is achieved towards higher voltages. Consequently, if the voltage exceeds the V_{max} limit of the inverter, the inverter stops and the Pmp is fully lost.

Vmin/Vmax Inverter Loss: If Vmp is outside of the inverter's window (Vmpmin/Vmpmax) the inverter will clip it to the limit value. This loss is the difference between P_{mp} and the corresponding P of the I-V curve at the limit value.

As seen in Fig. 10 when the diesel generator is requested to supply a load of around 20% of its nominal power, its consumption is very high (0.641 l/kWh). However, for heavy loads (higher than 80% of Pn) its consumption is equal to 0.324 l/kWh. Thus considerable fuel economies and a good efficiency may be obtained when the DG operates near this load fraction. These obtained results are in agreement with those obtained by other authors [35].

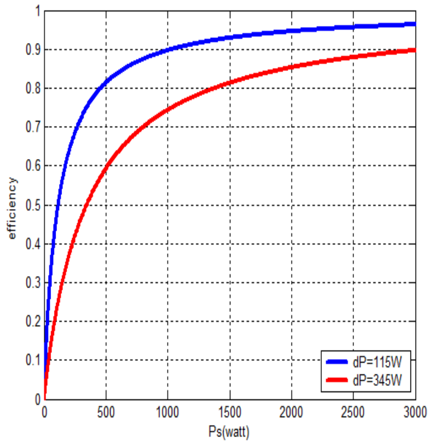

Figure 9: The efficiency of the inverter as function of the power demand

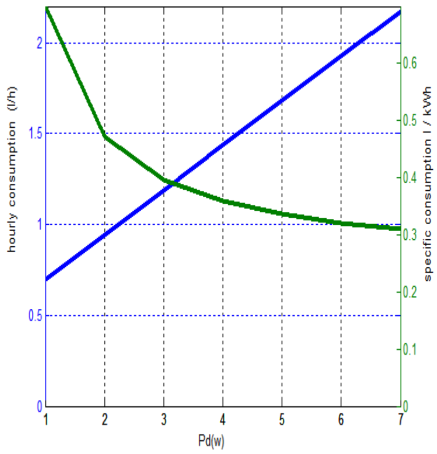

Figure 10: Consumption of the diesel generator as a function of the power produced

5. Summary/Conclusions

In the framework of this paper different components of a hybrid photovoltaic system were simulated following the proposed mathematical model depending on the meteorological conditions or the estimated data.

The results show that:

1. The P-V characteristic of the PV generator is nonlinear and changes with irradiation and temperature, and the PV generator performs a better in a low-temperature rather than at high-temperature environment.
2. The more slowly the battery is discharged, the more it is able to provide the necessary energy for the hybrid system.
3. Temperature has a great influence on battery performance: in discharge mode a temperature increase causes an increase in capacity, SOC and voltage, however, in charge mode the opposite is true.
4. The battery voltage is affected by temperature as is the SOC, for both cases of charge and discharge modes.
5. The manufacturers and the installers of such systems take into consideration the site and application (load profile) for which these pieces of equipments are intended in order to obtain a maximum efficiency.
6. The inverter must operate near its rated power for better performance.
7. Considerable fuel economies and a good efficiency may be obtained when the DG operates near its rated power.

For maximum efficiency of the entire system, it is necessary to establish an energy transfer management system that optimizes the operation of each component of the system while respecting their operating range. This will be the objective of a future work.

Indeed, the results can be used to give answers to many questions about this type of installation and to help manufacturers make the right decisions.

References

[1] W. Bifano, A. Ratajczak, D. Bahr, B. Garrett, Social and economic impact of solar electricity at schuchuli village.

[2] B. Bhandari, K.-T. Lee, G.-Y. Lee, Y.-M. Cho, S.-H. Ahn, Optimization of hybrid renewable energy power systems: A review, International Journal of Precision Engineering and Manufacturing-Green Technology 2 (1) (2015) 99–112.

[3] K. Reiniger, T. Schott, A. Zeidler, Optimization of hybrid stand-alone systems, in: European Wind Energy Association Conference and Exhibition, 1986.

[4] G. Contaxis, J. Kabouris, Short term scheduling in a wind/diesel autonomous energy system, IEEE Transactions on Power Systems 6 (3) (1991) 1161–1167.

[5] Klinghammer, W.; Norenberg, K.: Wide-scale village electrification with PV hybrid power systems in western China experience gained. 21st European Photovoltaic Solar Energy Conference,4-8 September 2006, Dresden, Germany, pp. 3023-3026, 2006.

[6] Tina, G.M., Brunetto, C., Gagliano, S., Petino, S., Guerra, M., Schioppo, R., Candio, A.: Monte Aquilone hybrid Photovoltaic-Diesel power generation system testing site-experimental tuning of subsystem models. 20th European Photovoltaic Solar Energy Conference, 6 –10 June 2005, Barcelona, Spain, pp. 2319-2322, 2005.

[7] Munoz, J., Narvarte, L., Lorenzo, E.: First operating year of two village PV-diesel plants in the south of Morocco. 19th European Photovoltaic Solar Energy Conference, 7-11 June 2004, Paris, France, pp. 3462-3465, 2004.

[8] C. W. Ajan, S. S. Ahmed, H. B. Ahmad, F. Taha, A. A. B. M. Zin, On the policy of photovoltaic and diesel generation mix for an off-grid site: East malaysian perspectives, Solar Energy 74 (6) (2003) 453–467.

[9] S. Rana, R. Chandra, S. Singh, M. Sodha, Optimal mix of renewable energy resources to meet the electrical energy demand in villages of madhya pradesh, Energy Conversion and Management 39 (3) (1998) 203–216.

[10] Oldach, R., Bates, J., Derrick, A., Gantulga, D., Hasnie, S., Enebish, N.: PV hybrid system for a remote village in Mongolia. 19th European Photovoltaic Solar Energy Conference, 7-11 June 2004, Paris, France, pp. 3540-3543, 2004.

[11] S. Shaahid, M. Elhadidy, Opportunities for utilization of stand-alone hybrid (photovoltaic+ diesel+ battery) power systems in hot climates, Renewable Energy 28 (11) (2003) 1741–1753.

[12] B. Wichert, M. Dymond, W. Lawrance, T. Friese, Development of a test facility for photovoltaic-diesel hybrid energy systems, Renewable energy 22 (1) (2001) 311–319.

[13] Suponthana, W., Ketjoy, N., Rakwichian W., Transforming solar home system to village grid system by using PV-farmer diesel hybrid system". 21st European Photovoltaic Solar Energy Conference, 4-8 September 2006, Dresden, Germany, pp. 3011-3015, 2006.

[14] M. Muselli, G. Notton, P. Poggi, A. Louche, Pv-hybrid power systems sizing incorporating battery storage: an analysis via simulation calculations, Renewable Energy 20 (1) (2000) 1–7.

[15] M. Ashari, C. Nayar, W. Keerthipala, Optimum operation strategy and economic analysis of a photovoltaic-diesel-battery-mains hybrid uninterruptible power supply, Renewable energy 22 (1) (2001) 247–254.

[16] Van Sark, W.G.J.H.M., Lysen, E.H., Cocard, D., Beutin, P., Merlo, G.F., Mohanty, B., vandenAkker, J., Razzak Idris, A., Firag, A., Waheed, A., Shaheed, A., Latheef, M., Wajeeh, A.: The first PV-diesel hybrid system in the Maldives installed at Mandhoo Island. 21st European Photovoltaic Solar Energy Conference, 4-8 September 2006, Dresden, Germany, pp. 3039-3043,2006.

[17] Vladimir Lazarov, Gilles Notton, Zahari Zarkov and Ivan Bochev.:Hybrid Power Systems with Renewable Energy Sources – Types, Structures, Trends for Research and Development. Proceedings of International Conference ELMA2005, Sofia, Bulgaria, pp. 515-520, 2005.

[18] Ludmil Stoyanov : Etude de différentes structures de systèmes hybrides à sources d'énergie renouvelables. Dissertation for the Doctoral Degree,Bulgaria: Universite Technique De Sofia, 2011.

[19] L. Stoyanov, G. Notton, V. Lazarov, Optimisation des systèmes multisources de production d'électricité à énergies renouvelables, Revue des énergies renouvelables 10 (1) (2007) 1–18.

[20] B. Wichert, Pv-diesel hybrid energy systems for remote area power generation—a review of current practice and future developments, Renewable and Sustainable Energy Reviews 1 (3) (1997) 209–228.

[21] S. Singer, B. Rozenshtein, S. Surazi, Characterization of pv array output using a small number of measured parameters, Solar Energy 32 (5) (1984) 603–607.

[22] M. G. Villalva, J. R. Gazoli, E. Ruppert Filho, Comprehensive approach to modeling and simulation of photovoltaic arrays, IEEE Transactions on power electronics 24 (5) (2009) 1198–1208.

[23] O. Gergaud, B. Multon, H. B. Ahmed, Analysis and experimental validation of various photovoltaic system models, in: ELECTRIMACS, 2002, p. 6p.

[24] G. Ciulla, V. L. Brano, V. Di Dio, G. Cipriani, A comparison of different one-diode models for the representation of i–v characteristic of a pv cell, Renewable and Sustainable Energy Reviews 32 (2014) 684–696.

[25] H. Tian, F. Mancilla-David, K. Ellis, E. Muljadi, P. Jenkins, A cell-to-module-to-array detailed model for photovoltaic panels, Solar Energy 86 (9) (2012) 2695–2706.

[26] M. Almaktar, H. A. Rahman, M. Y. Hassan, Effect of losses resistances, module temperature variation, and partial shading on pv output power, in: Power and Energy (PECon), 2012 IEEE International Conference on, IEEE, 2012, pp. 360–365.

[27] D. Sera, R. Teodorescu, P. Rodriguez, Pv panel model based on datasheet values, in: 2007 IEEE international symposium on industrial electronics, IEEE, 2007, pp. 2392–2396.

[28] J. Accarino, G. Petrone, C. Ramos-Paja, G. Spagnuolo, Symbolic algebra for the calculation of the series and parallel resistances in pv module model, in: Clean Electrical Power (ICCEP), 2013 International Conference on, IEEE, 2013, pp. 62–66.

[29] D. J. A. Jaleel, A. Nazar, A. Omega, Simulation on maximum power point tracking of the photovoltaic module using labview, International Journal of Advanced Research in Electrical, Electronics and Instrumentation Engineering 1 (3) (2012) 190–199.

[30] O. Gergaud, G. Robin, B. Multon, H. B. Ahmed, Energy modeling of a lead-acid battery within hybrid wind/photovoltaic systems, in: European Power Electronic Conference 2003, 2003, p. 8pp.

[31] Bendjamaa Ibrahim. : Modelisation et commande d'un système De stockage photovoltaïque. Dissertation for the Magister Degree ,Algeria: Universite Abou-Bakr Belkaid –Tlemcen, 2011.

[32] A. O. M. Yahya, A. O. Mahmoud, I. Youm, Modélisation d'un système de stockage intégré dans un système hybride (pv/eolien/diesel), Revue des énergies renouvelables 10 (2) (2007) 205–214.

[33] Bencherif Mohammed. : Modelisationlisation de systemmes énergétiques integration dans un système hybride photovoltaïques et eoliens basse tension. Dissertation for the Doctoral Degree ,Algeria: Universite Abou-Bakr Belkaid –Tlemcen, 2013.

[34] K. Kusakana, H. J. Vermaak, P. Jenkins, Hybrid diesel generator/renewable energy system performance modeling, Renewable energy (2013) 1–3.

[35] Daniel Yamegueu1, Yao Azoumah, Xavier Py.: Étude expérimentale et économique d'un système hybride solaire photovoltaïque diesel sans stockage pour une production décentralisée d'électricité. French Congress of Thermal / Solar Energy and Thermal / Perpignan, pp. 24-27 May 2011.

[36] Abdel Kadet Ould Mahmoud.: Caractérisation, modélisation, fonctionnement et impact d'un système hybride pour alimentation de charges mixtes. Dissertation for the Doctoral Degree, Senegal: Cheikh Anta-Diop University of Dakar, 2008.

[37] R. D. Grisso, M. F. Kocher, D. H. Vaughan, Predicting tractor fuel consumption, Applied Engineering in Agriculture 20 (5) (2004) 553–561.

[38] Herve Abdi. : The Method of Least Squares. In: Neil Salkind (Ed.) (2007). Encyclopedia of Measurement and Statistics.

[39] WH. Press, WT. Vettering and SA. Teukolsky. : Numerical Recipes in C: The Art of Scientific Computing. 2nd Ed. Cambridge University Press, Vol. 9, pp. 362 – 367, 2002.

[40] A. Dolara, R. Faranda, S. Leva, Energy comparison of seven mppt techniques for pv systems, Journal of Electromagnetic Analysis and Applications 2009.